Broadband Compact Substrate-Independent Textile Wearable Antenna for Simultaneous Near- and Far-Field Wireless Power Transmission

Mahmoud Wagih, *Member, IEEE*, Abiodun Komolafe, *Member, IEEE*,
Alex S. Weddell, *Member, IEEE*, and Steve Beeby, *Fellow, IEEE*

***Abstract*—Despite an increasing interest in wearable wireless power transmission (WPT), until now, wearable antennas have been unable to simultaneously harvest from near-field resonant and far-field radiative WPT. Here, a dual-port antenna is proposed, integrating an inductive coil with a broadband monopole for near- and far-field wearable WPT. The coil acts simultaneously as a High Frequency (HF) near-field power receiver and an Ultra-High Frequency (UHF) resonator, enabling the miniaturization of the enclosed broadband monopole, both fabricated using all-textile conductors. On-body, the antenna maintains a 10 dB return loss over a measured 135% fractional bandwidth while maintaining compactness ($0.312\times0.312\lambda^2$). The antenna is substrate-independent and is demonstrated on two textile substrates with different dielectric properties and thicknesses. In far-field mode, the rectenna maintains over 40% efficiency from sub-1 μW/cm^2 power densities. In the near-field, a WPT efficiency up to 80% can be achieved. The simulated Specific Absorption Rate (SAR) shows up to 40 and 20 dBm power reception for HF and UHF operation, respectively, without exceeding the 1.7 W/kg limit. The far-field wearable rectenna is demonstrated powering a Bluetooth Low Energy node using a BQ25504 DC-DC converter from a best-in-class low power density of 0.88 and 0.55 μW/cm^2 on-body and in-space, respectively.**

***Index Terms*—Antennas, Body Area Networks, Coils, Inductors, Rectennas, Rectifiers, NFC, RFID.**

I. Introduction

WIRELESS power transmission (WPT) and Radio Frequency (RF) Energy Harvesting (EH) are widely recognized as enablers of future sustainable Internet of Things (IoT) devices [1]–[3]. Wearable electronics and "e-textiles" in particular require flexible and body-friendly energy supplies to avoid cumbersome and unsustainable batteries [4], [5]. Leveraging the recent advances in wearable antennas realized using textile materials, a plethora of RF power harvesting rectennas have been demonstrated for wearable applications [6]–[9], including flexible rectennas integrated with textile-based energy storage [10], and textile rectennas for Simultaneous Wireless Information and Power Transfer (SWIPT) [11].

However, existing wearable rectennas will inevitably be limited in the DC power level they can generate, owing to human body absorption as well as the regulations on maximum Equivalent Isotropically Radiated Power (EIRP) and Specific Absoprtion Rate (SAR) levels [12]. Therefore, near-field magnetic resonance (MR) WPT has been widely investigated using flexible and textile materials, for efficient WPT over a few milliwatts [13]. However, with a maximum range of a few centimeters for most wearable MR-WPT coils [13], MR-WPT cannot solely provide wearables with the full spatial freedom promised by radiative WPT. To date, there has been no report of a wearable rectenna operating as a simultaneous near-field High Frequency (HF) and far-field Ultra-High Frequency (UHF) power receiver.

Near-field HF and far-field UHF functionalities have previously been integrated in a single device for Radio Frequency Identification (RFID) applications [14]–[17]. Using dual-mode near/far-field antennas, IoT devices can be powered using magnetic resonance (MR) power transfer as well as far-field radiative WPT. Furthermore, Near Field Communication (NFC) and UHF RAIN$^{\text{TM}}$ RFID can be simultaneously used for connectivity. In [17], a tightly packed monopole antenna was proposed alongside an NFC coil on the same Printed Circuit Board (PCB), the UHF antenna maintained a matched S_{11} around 0.9 and 2.4 GHz, covering both license-free bands, yet, both elements operated independently with no means of improving the antenna's performance using the coil's area. A circularly-polarized single-port antenna was also proposed for near HF and far-field UHF RAIN$^{\text{TM}}$ RFID applications [16]. Despite achieving a relatively wide 3 dB axial ratio bandwidth covering the sub-1 GHz RFID band, the antenna's bandwidth was limited to 15.7%. To explain, despite UHF/Ultra-Wide Band (UWB) antennas previously being implemented [18], there has been no report of a broadband antenna integrated with a near-field HF element.

Therefore, existing HF coil/UHF antenna integration efforts do not demonstrate the feasibility of using a shared aperture coil/antenna for broadband (>100%) fractional bandwidth applications, or show the potential for miniaturizing the antenna using the coil's area. Furthermore, no wearable dual-mode near and far-field antenna has been reported, for either communication or power transmission applications. To explain, the

This work was supported by the UK Engineering and Physical Sciences Research Council (EPSRC) under Grant EP/P010164/1 and the European Commission through the EnABLES Project grant number: 730957. M. Wagih was supported by the UK Royal Academy of Engineering and the Office of the Chief Science Adviser for National Security under the UK Intelligence Community Post-Doctoral Research Fellowship programme. S. Beeby was supported by the UK Royal Academy of Engineering under the Chairs in Emerging Technologies scheme. (*Corresponding author: Mahmoud Wagih*)

The authors are with the School of Electronics and Computer science, University of Southampton, Southampton, SO17 1BJ, U.K. (email:mahm1g15@ecs.soton.ac.uk)

Digital Object Identifier: , datasets used in this paper will be made available from the University of Southampton repository at DOI: X

existing near/far-field antennas do not address the wearable-specific challenges including: (a) on-body detuning, (b) UHF radiation efficient degradation, (c) compatibility with different and often too lossy and electrically-thin fabric substrates, and (d) compliance with the SAR regulations.

In this paper, we propose a dual-port inductor-loaded broadband antenna for wearable near- and far-field power reception in the HF and the UHF license-free bands, with with a measured 135% fractional bandwidth. The key contributions of the work can be summarized as:

1) presenting the first broadband antenna integrated with a near-field coil for HF operation, and the first dual-band/mode near- and far-field wearable antenna;
2) utilizing the HF coil as a resonator for miniaturizing the monopole to less than 80% of the area of a conventional disc monopole covering the same bandwidth, while adding HF connectivity;
3) realizing a compact wearable broadband antenna with a stable bandwidth on the body, transferable to different textile substrates of different thicknesses and ϵ_r;
4) demonstrating a high near-field coupling and high far-field gain at each port with over 20 dB isolation in the license-free bands, along with an SAR of less than 1.7 W/kg for operation at 100 mW and 10 W for near and far-field power harvesting.
5) demonstrating, for the first time, a wearable rectenna, not isolated from the body, powering a real load using a commercial DC-DC converter from a sub-1 μW/cm^2 power density.

In Section II, the antenna design and simulation process is presented. Section III then reports the antenna's fabrication and characterization, with the near and far-field power transmission performance presented in Section IV.

II. Antenna Design and Simulation

In order to receive wireless power in the UHF spectrum, the antenna's bandwidth needs to cover the license-free bands in which power can be delivered [19]. For an efficient wearable antenna to be realized on lossy textile materials while maintaining a low thickness, an unisolated monopole antenna is selected because:

1) A thinner, more flexible, and more efficient (due to the reduced susbtrate and conductor losses) antenna could be realized below 1 GHz as decoupling the antenna from the body using a ground plane cannot be done using an "electrically-large" structure [20]. This is demonstrated numerically against a standard microstrip patch on the same textile substrate in Section III-C.
2) An unshielded monopole could maintain a wide bandwidth, making the antenna immune to on-body detuning and also transferable to substrates with a different thickness and permittivity.
3) In energy harvesting from arbitrary directions, omnidirectional sub-1 GHz on-body monopoles outperform their 2.4 GHz directional counterparts owing to their wider beam-width [21].
4) Body-induced losses were found to not reduce the RF-to-DC efficiency of wearable far-field rectennas, despite having no isolation from the body and a gain under 0 dBi [8], [9].

Therefore, the rectenna is designed based on an omnidirectional "wire-type" antenna, covering the 868/915 MHz license-free bands. It was previously shown that omnidirectional antennas are suitable for low-power energy harvesting on the body with a stable S_{11} response [8], [9].

While energy harvesting antennas can be designed to directly match the input impedance of the rectifier with no intermediate matching stage [3], [22], [23], designing the antenna to match a 50 Ω characteristic impedance offers more flexibility with the rectifier design and enables the antenna to be connected to different rectifiers covering multiple bands [3]. Furthermore, high sensitivity rectifiers have been realized on textile substrates using lumped components with over 40% Power Conversion Efficiency (PCE) at -20 dBm [9], surpassing that of rigid rectifiers on low-loss substrates [24]. Broadband antennas have the additional advantage of not detuning in human proximity, where they can maintain a 50 Ω $S_{11} < -10$ dB over different body positions [9], [25].

The antenna design steps are:

1) Scaling a broadband (>100% bandwidth) antenna to the sub-1 GHz spectrum.
2) Miniaturizing the antenna for integration within the coil, i.e. rectangular resonator.
3) Designing the surrounding HF coil with an inner diameter over λ/4 (λ for the UHF bandwidth) to act as a coupled resonator for antenna miniaturization.
4) Optimization of the UHF antenna feed to remove the dependency on the substrate's height and permittivity.

First, a scalable UWB-inspired design is used, which enables a fractional bandwidth over 100% covering the sub-1 GHz bands. The antenna is first based on the circular disc monopole [26], widely used to realize broadband antennas with microstrip and Coplanar-Waveguide (CPW) feeds [27]. Step 1 in Fig. 1 shows the layout and dimensions of the simple disc monopole, where the lower end of the impedance bandwidth is primarily controlled by the diameter of the disc D_1 [9], [26].

The UWB-inspired disc antenna was simulated in CST Microwave Studio to observe its impedance bandwidth from 0.5 to 4 GHz. The antenna has been simulated using a lossy copper model and a substrate of ϵ_r=1.2 and tanδ=0.023, matching that of felt, which is typically in the region of 1.03 to 1.2 [9], [11], [24], widely-used as a wearable antenna substrate. Fig. 2(a) shows the simulated reflection coefficient of the antenna for varying disc radii. Based on the simulated response, an antenna with an area of 140$\times$100 mm is needed for the S_{11} bandwidth to cover the 868/915 MHz band. The simulated parameters of the antenna at each design step are summarized in Table I.

It was previously shown that an elliptical [27] as well as a half-disc monopole [28], can maintain a broad bandwidth comparable to that of the standard disc. The monopole antenna is subsequently miniaturized by omitting half of the disc and

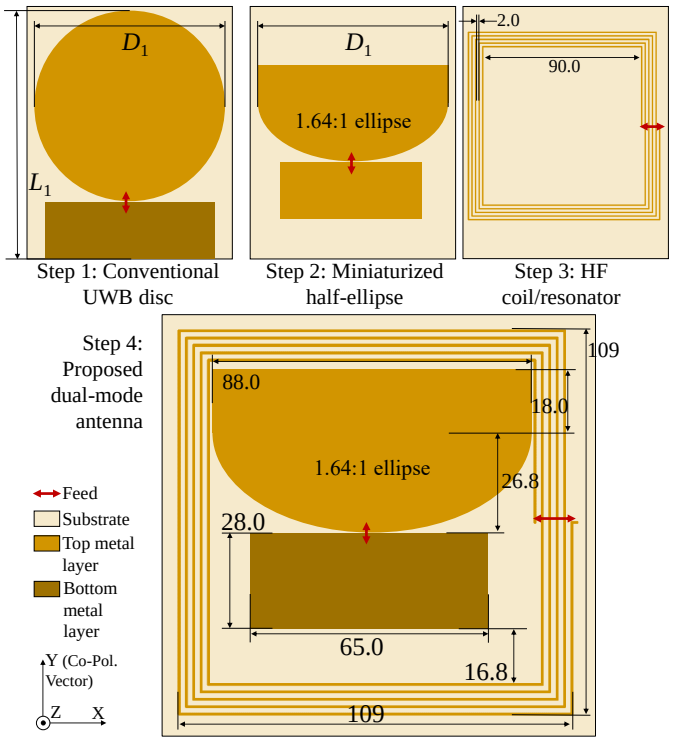

Fig. 1. Design steps of the proposed antenna showing its layout and dimensions (in mm).

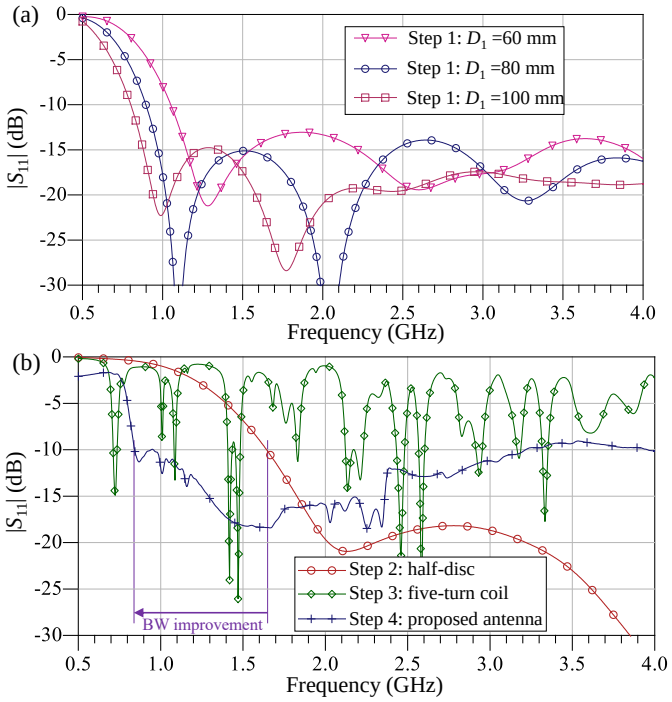

Fig. 2. Simulated reflection coefficient of the antenna at different design steps: (a) conventional broadband disc with different radii [26]; (b) the miniaturization of the antenna using a multi-turn coil as a rectangular resonator.

TABLE I
THE ANTENNA'S PARAMETERS AT 900 MHZ FOR EACH DESIGN STAGE.

	S_{11} $<$ -10 dB BW (GHz)	Rlz. gain at 900 MHz	Total η at 900 MHz	Dimensions (mm)
Step 1: disc D_1=100 mm [26], [29]	0.80–4.0	2.45 dBi	>95%	140× 100
Step 2: miniaturized disc	1.44–4.0	−3.4 dBi	28.2%	88× 71
Step 3: stand-alone coil	none	1.62 dBi*	68%†	109× 109
Step 4: dual-mode antenna	0.8–4.0	2.49 dBi	79.4%	109× 109

*IEEE Gain (exclusive of mismatch); †Radiation η (exclusive of mismatch)

adding a rectangular section to increase the antenna's lower bandwidth, as shown in Step 2 in Fig. 1. The disc is then scaled to create an ellipse with a 1.64:1 horizontal to vertical ration. In addition, the size of the ground plane has been reduced from 110×28 to 65×28 mm. The simulated S_{11} of the miniaturized antenna is shown in Fig. 2(b), where it can be observed that the antenna now maintains an S_{11} bandwidth from 1.7 GHz as opposed to approximately 0.9 GHz. This in turn reduces the antenna's total efficiency in the sub-1 GHz spectrum, resulting in a lower gain as shown in Table I.

To enable the antenna to operate as a dual-mode near- and far-field power receiver, a near-field HF resonant coil is needed. Furthermore, by loading the antenna using the coil, which acts as a resonator in the UHF spectrum, the UHF antenna's radiator size can be miniaturized. To explain, the use of single-loop coupled resonators including rectangular [19] and ring resonators [30] has previously been reported for miniaturizing dipole antennas. As a result, the near-field HF WPT coil is proposed as a loading-element which enables the miniaturization of the broadband UHF radiator. Fig. 2(b) shows the S_{11} of the miniaturized antenna, step 4 in Fig. 1, when loaded with a 5-turn coil. The UHF radiating element is fully-enclosed by the coil as opposed to having an electrical ground which extends beyond the coil. To explain, the overlap of the coil's conductors with the ground plane of a monopole microstrip feed introduces a non-uniform current in the ground plane which in turn degrades the antenna's matching.

In addition to maintaining a stable S_{11} bandwidth on the body, a broadband antenna with a very short microstrip feed can be ported to different textile substrates without the need to re-design the antenna. To explain, to implement a conventional microstrip patch antenna on different textile substrates, prior knowledge of the thickness and dielectric properties of the fabric is needed [31]. On the other hand, a broadband monopole antenna will be expected to maintain its bandwidth despite small variations in the relative permittivity as well as the height of the substrate, where most textiles have an ϵ_r <3.0 [24]. To demonstrate the antenna's matched bandwidth over the human body as well as on different textile substrates, the antenna was simulated using using the dielectric properties of two textile substrates: 1 mm-thick felt with ϵ_r=1.2 and tanδ=0.023 [9], and 0.44 mm-thick polyester cotton with ϵ_r=1.7 and tanδ=0.017 [32]. On both substrates, the simulated $|S_{11}|$ response was similar, and is investigated experimentally on both substrates in the next section.

A simplified layered tissue model was used to observe the

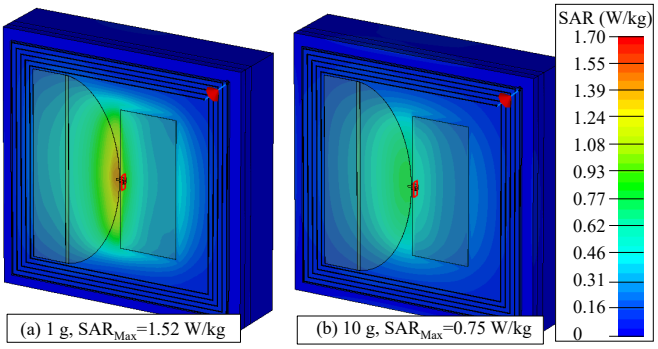

Fig. 3. Simulated SAR of the antenna at 900 MHz for a 20 dBm input: (a) averaged over 1 gm tissue mass; (b) averaged gm tissue mass.

antenna's performance near the body, as well as calculate the antenna's SAR when operating as a far-field power receiver. As the antenna is not decoupled from the body using a ground plane or a reflector, the SAR calculation is of paramount importance to demonstrate the antenna's safety for on-body use. The SAR was calculated for a 20 dBm (100 mW) RF input at 900 MHz, which represents a higher limit for the amount of power the antenna may receive from a standard license-free transmitter with a 4 W EIRP limit. The simulated peak SAR plots are shown in Fig. 3(a) and (b) averaged over 1 and 10 gm tissue mass, respectively. It can be observed that the proposed antenna complies with the IEEE C95.1 1.7 W/kg limit. As for MR-WPT, it was previously shown that an SAR under 0.2 W/kg is maintained for two rectangular coils transferring power through the body at optimal coupling [13], owing to the low absorption of human tissue in the HF spectrum.

III. Antenna Fabrication and Measurements

A. Hybrid E-Textile Fabrication

The proposed antenna has been realized using two e-textile fabrication methods. The UHF antenna, being a large-area component, can be realized using screen-printed laminated conductors [32] or commercially-available conductive fabrics [6], [11]. A copper and nickel conductive fabric from P&P (MetWeave), with a sheet resistance under 0.1 Ω/square, was used for the UHF antenna's radiating elements. The antenna's patterns were cut using a Graphtec robo-cutter and attached onto the fabric using the fabric's adhesive backing. This fabrication method can be automated using on-textile moulds, which have previously been used to realize multi-layered microstrip antennas on textiles [33].

Embroidered coils based on Litz threads were previously found to have the highest wireless power transfer efficiency compared to other printed and flexible e-textile coils, owing to their lower resistance compared to printed conductors [13]. The 5-turn coil was fabricated using silk-coated Litz threads of 40 µm thickness, embroidered onto the same substrate using a PFAFF creative 3.0 embroidery machine. The antenna has been realized on both the 1 mm-thick felt and 0.44 mm-thick polyester cotton substrates. Fig. 4(a)-(c) show photographs of the proposed antenna, with the embroidered coil and rectifier micrographs shown in Fig. 4(d) and (e).

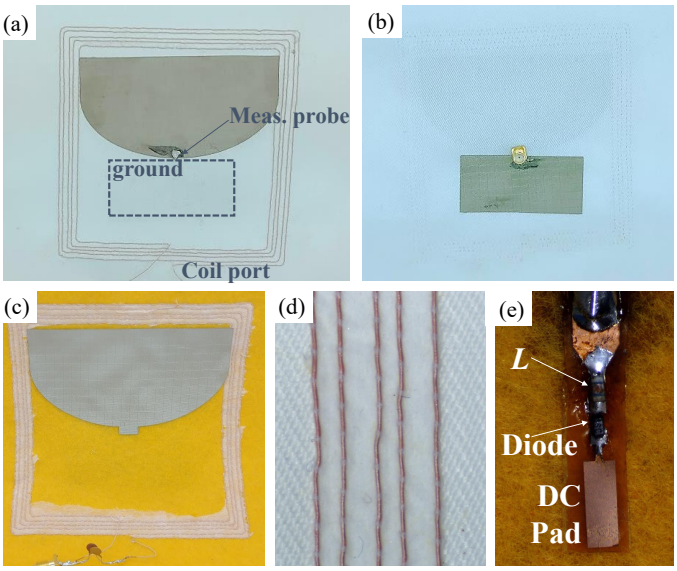

Fig. 4. Photographs of the fabricated antenna: (a) antenna's top layer on the poly-cotton substrate; (b) antenna's bottom layer; (c) the antenna's top layer on a felt substrate; (d) micrograph showing the over-stitched coils; (e) micrograph of the rectifier realized on a flexible polyimide filament bonded to the rough felt substrate.

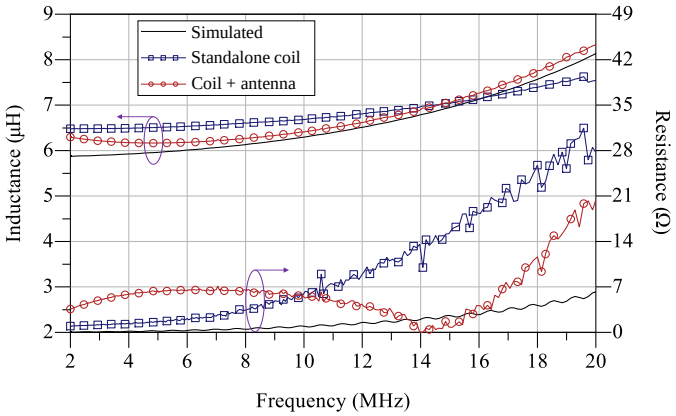

Fig. 5. Simulated and measured inductance and resistance of the coil before and after the UHF radiating elements are added.

B. HF Coils Characterization

The input impedance of the realized textile coils has been measured using a Rohde & Schwarz ZVB4 Vector Network Analyzer (VNA) to evaluate their inductance as well as series resistance. SMA connectors were soldered onto the coils' terminals to measure their S_{11} parameters using the VNA. Fig. 5 shows the full-wave simulated inductance of the coil as well as the measured inductance and resistance of the fabricated coil. The inductance was calculated from the simulated (using a lumped/discrete port) and measured $\Im\{Z_{11}\}$ as L=$\Im\{Z_{11}\}/(2\pi f)$. Both coils, implemented on the felt and polyester cotton substrates, exhibited a similar Z_{11} within 2%; only one plot is shown in Fig. 5.

Observing Fig. 5, it can be seen that the fabricated coils maintain a stable inductance in the 6.78 MHz band, with a self-resonant frequency over 20 MHz. Furthermore, it can be observed that the unloaded coil maintains a very low

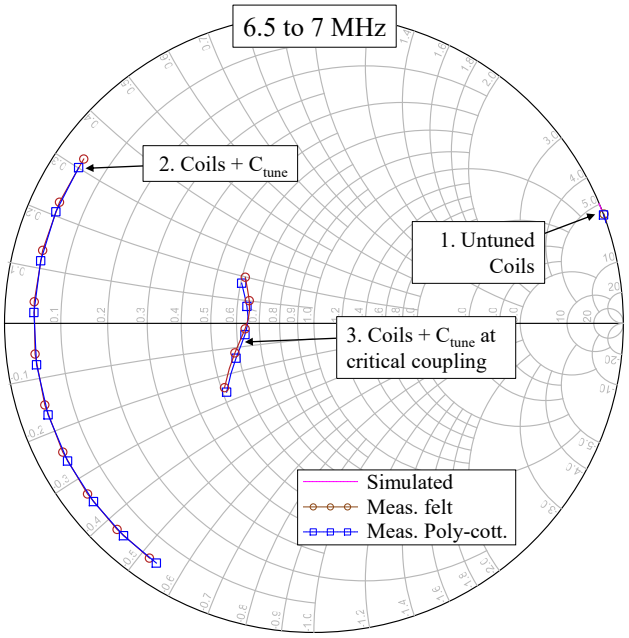

Fig. 6. Smith chart plot of showing the input impedance of the coils before and after capacitive tuning, as well as at critical coupling.

loss resistance. At 6.78 MHz, before the UHF radiating element is attached, the coil maintains a Q-factor over 120 (Q=$\Im\{Z_{\rm in}\}/\Re\{Z_{\rm in}\}$). The inclusion of the UHF radiating elements results in an increase in the series resistance at 6.78 MHz to around 7 Ω, resulting in a lower Q-factor of 41 at 6.78 MHz. This can be attributed to the additional losses in the conductive fabric forming the antenna, which approach the inner turns of the coil where a high E and H-field density is maintained.

To achieve resonance at f_r=6.78 MHz, the coils were tuned using a series capacitor $C_{\rm tune}$, whose value is given by

$$C_{\rm tune} = L \times (2\pi f_r)^2, \tag{1}$$

where L is the measured inductance of the coil. For the measured L=6.2 μH, the calculated $C_{\rm tune}$ is 88.9 pF, realized using 53 and 36 pF lumped ceramic capacitors, soldered directly on the SMA/coil interface for VNA measurements. Small footprint high-Q RF surface-mount capacitors can be easily integrated on a compact flexible circuit filament, as with the UHF rectifier's matching network. Alternatively, an all-flexible HF power receiver can be realized using printed microwave textile-based capacitors, demonstrated up to 50 GHz [32], which can be scaled to values over 40 pF with a self-resonance in the GHz range.

The coil tuning is visualized on the Smith chart in Fig. 6. The simulated and measured (predominantly imaginary) impedance of the coils overlap, with the tuned coils exhibiting a very similar $Z_{\rm in}$ response on both substrates. When two symmetric coils are in close proximity at the critical coupling distance, $Z_{\rm in}$ approaches 50 Ω resulting in a high S_{21} between the coils. The WPT efficiencies and coupling between the coils are further explored in Section IV-C.

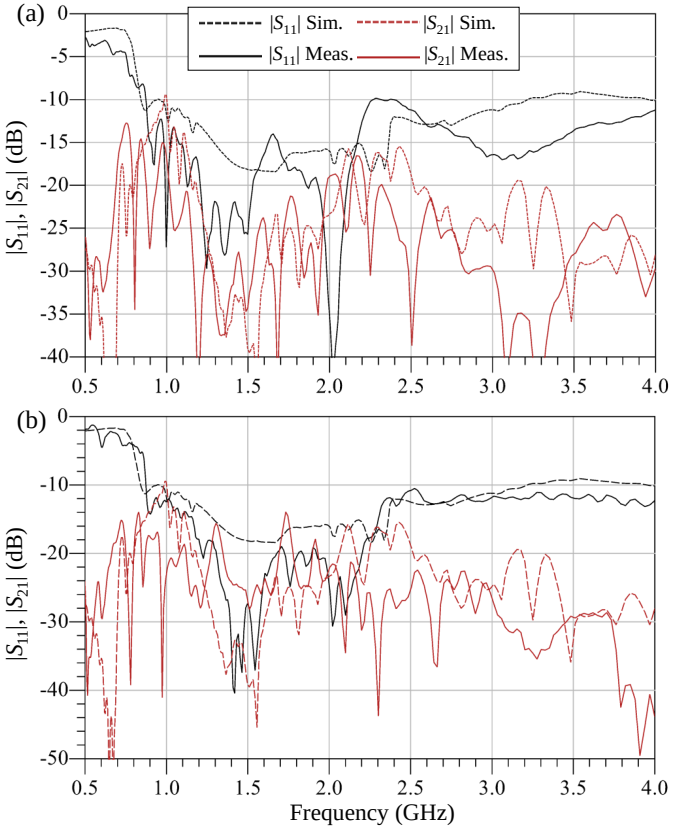

Fig. 7. Simulated (dashed) and measured (solid) reflection coefficient and port-coupling of the antenna on two textile substrates in the UHF spectrum: (a) 0.45 mm-thick polyester cotton substrate; (b) 1 mm-thick felt substrate.

C. UHF Antenna Characterization

The first step in characterizing the antenna's UHF properties is measuring its impedance bandwidth. Fig. 7 shows the simulated and measured reflection coefficient $|S_{11}|$ of the antenna, as well as the mutual coupling ($|S_{21}|$) between the near-field (MR-WPT coil) and far-field (rectenna) ports.

Observing both Fig. 7(a) and (b), it can be observed that the antenna maintains an $S_{11} < -10$ dB bandwidth starting from 800 MHz, in agreement with the simulated response. Furthermore, the bandwidth is maintained over the two different substrates, despite having different thicknesses and dielectric properties. This demonstrates the suitability of the proposed antenna for different fabrics without the need to re-measure their dielectric properties or re-design the antenna's radiator or feed. In addition to the matched S_{11}, both fabricated prototypes exhibit under -15 dB mutual-coupling for most of the impedance bandwidth.

In addition to maintaining their bandwidth on two different substrates, the antennas need to be characterized in human proximity as well as under bending. Both antennas have been placed on the user's chest, as well as bent around the E and H-planes with a radius of 4 cm. Fig. 8 and 9 show the masured s-parameters of the antenna under bending and on-body, for the woven polyester cotton and felt substrates, respectively, as well as the simulated response on the layered body model. The matched $|S_{11}|$ response over both substrates demonstrates that

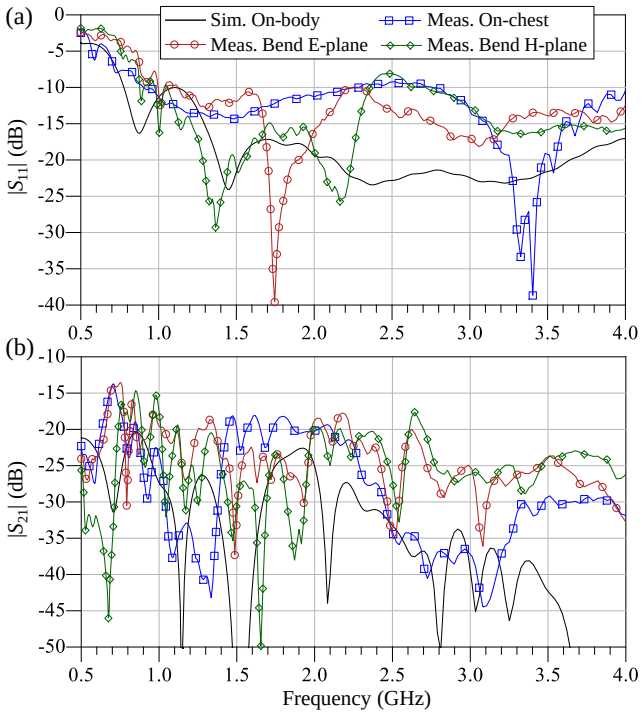

Fig. 8. Simulated and measured s-parameters of the antenna, on a polyester cotton substrate, on-body and under bending: (a) reflection coefficient; (b) ports' mutual-coupling.

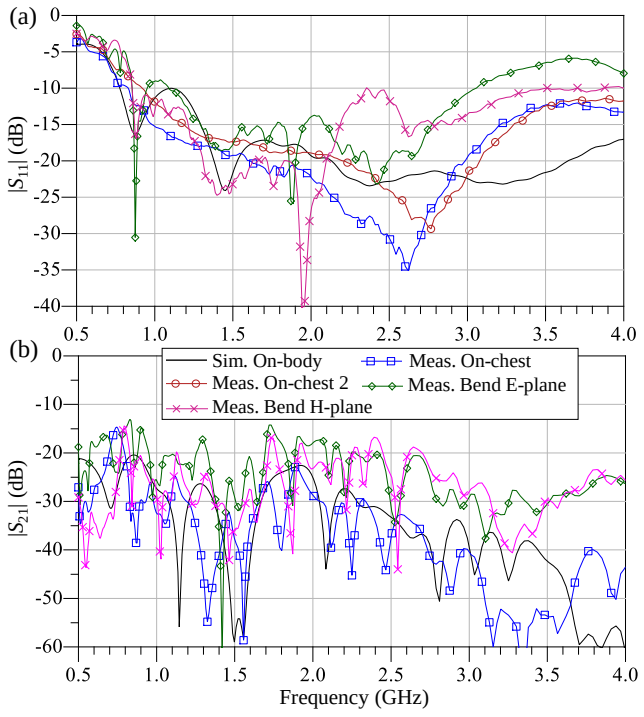

Fig. 9. Simulated and measured s-parameters of the antenna, on a felt substrate, on-body and under bending: (a) reflection coefficient; (b) ports' mutual-coupling.

the antenna is suitable for wearable applications, exhibiting a high immunity to bending and human proximity, which is a further advantage of using a broadband antenna for wearable applications.

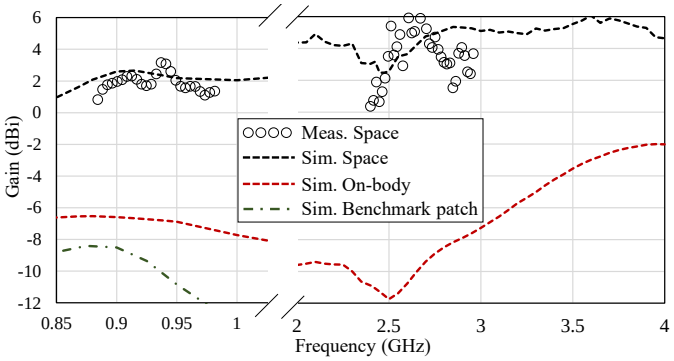

Fig. 10. Simulated and measured realized gain of the proposed antenna, around the sub-1 GHz and 2.4 GHz license-free bands; the direction of the peak gain is maintained in the broadside direction, i.e. θ=0°.

The radiation patterns of the proposed antenna were simulated in CST Microwave Studio as well as measured experimentally. Fig. 10 shows the simulated and measured realized gain of the antenna, around the license-free bands of 868/915 MHz as well as 2.4 GHz, and through to the lower end of the UWB spectrum. The gain was measured using a reference antenna in line-of-sight, in the far-field of both antennas, with the path loss calculated using the Friis formula. As observed in Fig. 10, the antenna maintains a stable gain across its bandwidth. Although the measured gain, using the free-space loss and a reference antenna, exhibits some fluctuations attributed to the additional reflections in the measurement setup, it mostly correlates to the simulated gain, indicating that the antenna is suitable for operation in the sub-1 GHz and 2.4 GHz license-free bands.

A key advantage of the proposed low-profile antenna, with no electrical shielding from the human body, is its ability to maintain a high radiation efficiency on an electrically-thin substrate [20], with several on-body harvesters demonstrated with no shielding at 433 MHz [34], 800 MHz [9], and 2 to 4 GHz [8]. To explain, the polyester cotton substrate used in this work with a 0.44 mm thickness ($0.0013\times\lambda_0$ at 900 MHz) is too thin to support an efficient microstrip antenna or Artificial Magnetic Conductor (AMC)-backed textile antenna [35]. To demonstrate that an unshielded monopole will be the most efficient radiation below 1 GHz with such a thin substrate, a standard TM01 microstrip patch with L=115 mm and W=150 mm was simulated in CST using the same substrate dielectric properties for benchmarking. The antenna was matched using a microstrip stub to maintain $S_{11} < -10$ dB.

In the absence of a human phantom, the microstrip patch maintains a radiation efficiency of -15.7 dB (i.e. 2.7%), and a peak gain of -8.4 dBi, plotted in Fig. 10 alongside the gain of the proposed antenna. While the gain of both the microstrip patch and the proposed monopole (in human proximity) are comparable, the proposed antenna maintains a higher simulated efficiency of 10%, a four-fold improvement over a conventional patch on the same substrate. It was previously shown that the radiation efficiency as opposed to the gain is the main figure-of-merit in RF energy harvesting and WPT from arbitrary directions [36]. Moreover, when considering

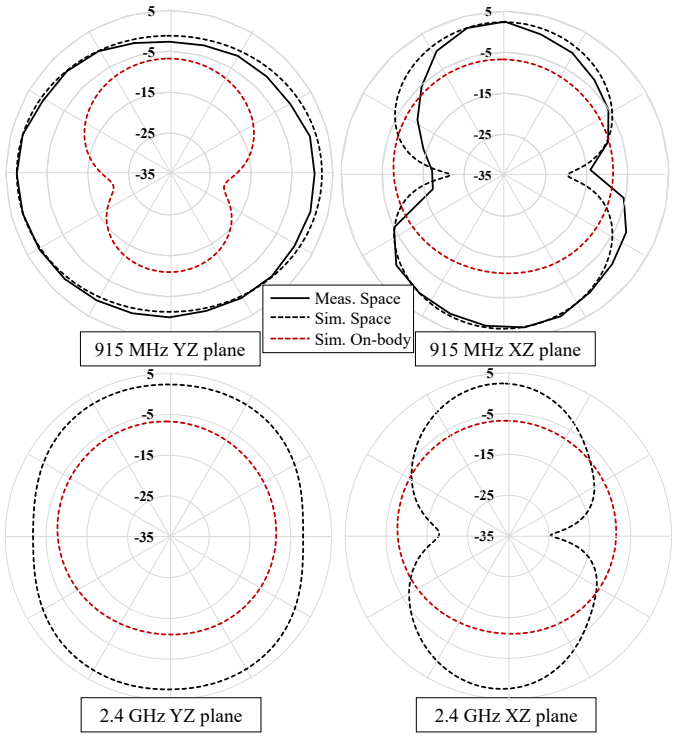

Fig. 11. Simulated and measured gain patterns of the proposed antenna in space and on the layered body model at 915 MHz and 2.4 GHz.

the physical footprint of both antennas, the proposed antenna occupies around 14% less area than the microstrip patch, in addition to having the ability to operate as a near-field receiver.

The elevation patterns of the antenna were measured experimentally over both the YZ and XY planes (from Fig. 1) at 915 MHz, as well as simulated over the antenna's S_{11} bandwidth. From the simulated and measured patterns, shown in Fig. 11, it can be observed that the antenna maintains omnidirectional radiation patterns, with a 360° half-power beam-width over the YZ plane. Moreover, the direction of the antenna's peak gain is maintained up to 4 GHz. As for the simulated patterns on the tissue model, the antenna exhibits a broadside off-body beam with a wider beam-width.

IV. Near and Far-Field Power Harvesting Measurements

A. UHF Sub-1 GHz Rectenna Evaluation

To realize a sub-1 GHz high-sensitivity rectenna, the proposed antenna is integrated with a miniaturized high-efficiency textile-based rectifier. The rectifier is based on the low-barrier Skyworks SMS7630 Schottky diode, chosen for its low forward voltage of around 140 mV for a 0.1 mA current draw. The detailed design process of the microstrip rectifier's layout is in [9]. The rectifier has been fabricated and integrated on the same felt substrate as the antenna. The PCE of the rectifier was characterized using a 50 Ω VNA configured as a Continuous Wave (CW) generator, and simulated using harmonic balance simulation in Keysight ADS, using the datasheet parameters and the packaging parasitics, previously shown in [9]. The

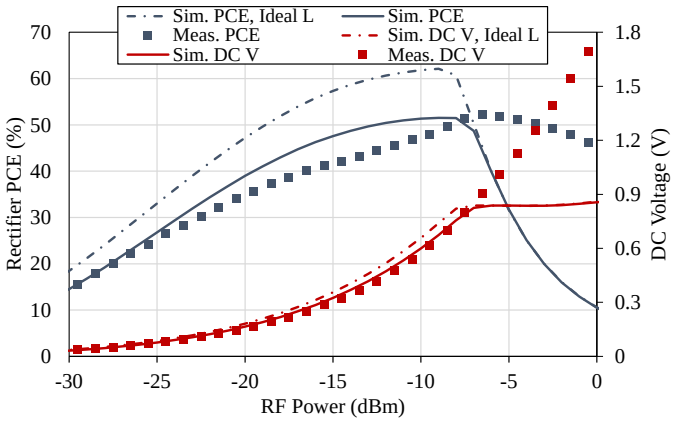

Fig. 12. Simulated (using an ideal and real inductor) and measured PCE and DC voltage output of the rectifier at 900 MHz using a 50 Ω source.

simulated and measured PCE and DC voltage output, across the optimum load of 7 kΩ, are shown in Fig. 12.

Owing to the very low forward voltage drop of the SMS7630 diode, as well as the impedance matching of the rectifier specifically tuned for low power levels, a high PCE surpassing 35% is achieved at −20 dBm. The effect of the resistive losses in the lumped inductor are also illustrated in Fig. 12, which reduce the achievable peak PCE by over 20%. Nevertheless, the use of a lumped inductor is essential to realize the high input impedance required by the diode, maintain a very compact rectifier layout, and avoid the high insertion losses should a distributed element matching network be realized on the lossy (tanδ >0.017) textile substrates.

To observe the effect of varying the load impedance on the rectifier's PCE, the load was swept from 100 Ω to 100 kΩ. Fig. 13 shows the simulated and measured PCE and DC voltage output, at −20 and −10 dBm, for the loads considered, where it can be observed that up to 42% PCE can be achieved at −20 dBm. The optimum load impedance range between 4 and 8 kΩ is in-line with recently reported boost converters aimed at RF energy harvesting applications [24], showing that the DC output of the proposed rectifier down to −20 dBm is suitable for powering a system with a 1 V output, when integrated with the aforementioned boost converter in [24].

To integrate the antenna with a single-series rectifier, a DC current return path is needed through the antenna [9]. A conductive Litz thread has been added to connect the antenna's ground plane to the radiating element. Fig. 14 shows the impedance of the antenna around the sub-1 GHz band after the addition of the shorting wire, which does not affect the antenna's S_{11} bandwidth.

After integrating the antenna with the rectifier, the overall rectenna's wireless power harvesting efficiency can be characterized. The VNA, configured to act as a CW generator, has been connected to a Mini-Circuits ZHL-4240W+ power amplifier (PA) with up to 41 dB small-signal gain and a 31 dBm 1 dB compression output. The output of the PA is fed into a directional Yagi-Uda antenna with an 8.8 dBi gain, through a 3 dB attenuator to mitigate any Voltage Standing Wave Ratio (VSWR) variations with the antenna's setup.

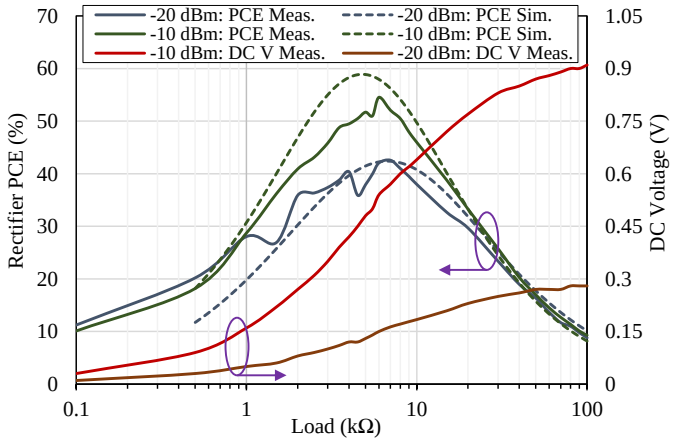

Fig. 13. Simulated and measured PCE and DC voltage output as a function of the load at 900 MHz.

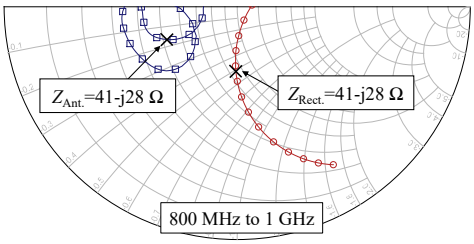

Fig. 14. Measured input impedance of the antenna, after adding the DC current return path, and the non-linear HB-simulated impedance of the rectifier.

As the PA's response is non-linear near its saturation limit, the VNA's second port was used to measure the forward transmission between the transmitter and the textile antenna (with a 50 Ω SMA port), to quantify the power available for the rectenna relative to the VNA's signal source output, as shown in step 1 in Fig. 15. Following the S_{21} measurement, at different power levels, the connectorized antenna is replaced with the rectenna, whose DC voltage output is monitored using an oscilloscope. Fig. 16 shows the measured DC output and wireless PCE of the antenna for varying input power levels from the CW source.

To quantify the antenna's sensitivity, the incident power density S is calculated as

$$S = \frac{P_{\mathrm{TX}} G_{\mathrm{TX}}}{4\pi d^2}, \tag{2}$$

where P_{TX} is the estimated input to the antenna after the PA and attenuators, G_{TX} is the antenna's gain, and d is the 2 m separation, satisfying the Fraunhofer far-field condition. The rectenna's wireless PCE is then calculated as

$$\mathrm{PCE}_{\mathrm{Rectenna}} = \frac{P_{\mathrm{DC}}}{P_{\mathrm{CW}} \times |S_{21}|^2}, \tag{3}$$

where P_{DC} is the rectifier's DC output, P_{CW} is the power level of the VNA's CW source, and $|S_{21}|$ (linear dimensionless) is the measured forward transmission between the transmitter and the reference connectorized textile antenna, used for estimating the received power.

Observing the measured efficiency of the integrated rectenna, in Fig. 16, it can be seen that the PCE is lower

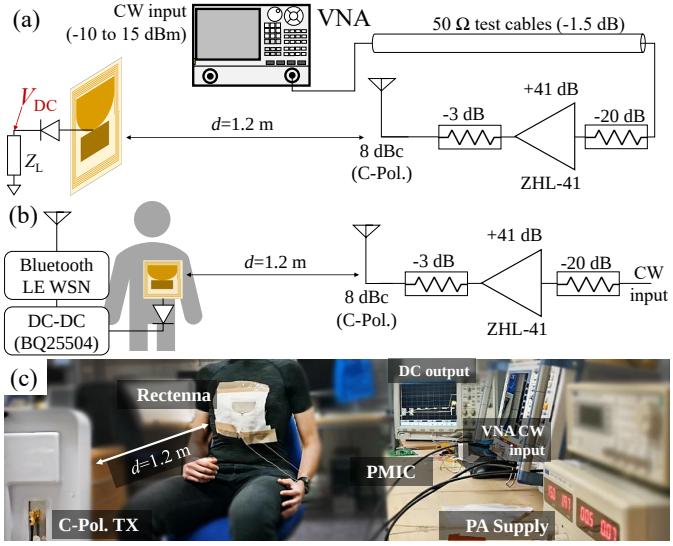

Fig. 15. Measurement setup of the proposed rectenna showing: (a) DC output characterization under varying S; (b) on-body setup with a DC-DC PMIC and a real load; (c) photograph of the on-body setup.

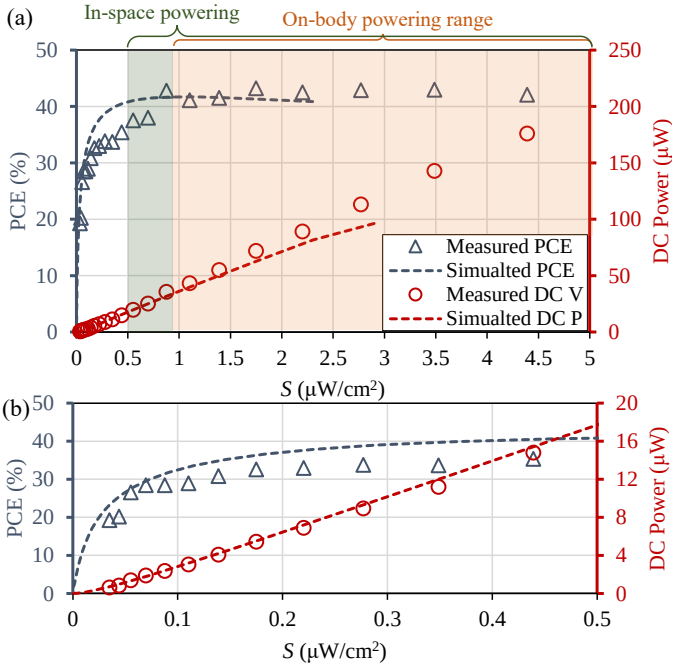

Fig. 16. Simulated and measured wireless PCE and DC output of the proposed rectenna at 900 MHz for a 7 kΩ load: (a) 0.05–5 μW/cm^2 power densities; (b) the sub-0.5 μW/cm^2 region.

than that achieved using an ideal 50 Ω source, in Fig. 12. This is attributed to the antenna's impedance not exactly matching 50 Ω. The additional impedance mismatch between the antenna and the rectifier is illustrated in Fig. 14, where it can be seen that both the antenna and the rectifier have a small capacitive imaginary impedance component, and the antenna's real impedance at 900 MHz approaches 25 Ω, whereas the rectifier's $\Re\{Z\}$ is close to 40 Ω.

The rectifier's PCE has been re-simulated using a port impedance matching that of the antenna, shown on the Smith

chart in Fig. 14. In Fig. 16, it can be seen that the simulated PCE of the antenna below 0.5 μW/cm^2 is still over 40%, which demonstrates its suitability for high-sensitivity RF power harvesting with comparable performance to rectifiers implemented on both textile and rigid substrates using the same diode [7], [24]. In Fig. 16, the power densities at which a commercial DC-DC converter can be charged to successfully power a low-power Wireless Sensor Node (WSN) are shown for measurements carried out in the presence (on-body powering) and absence (in-space powering) of the human body; the DC-DC charging is detailed in the next sub-section.

B. DC-DC Converter Integration and On-Body Powering

While several wearable rectennas have been reported [6]–[9], their on-body DC output has not been used to power a real load or demonstrate their ability to integrate with a commercial DC Power Management Integrated Circuit (PMIC). The proposed rectenna is integrated with a commercial PMIC based on the Texas Instruments (TI) BQ25504, which contains a DC-DC boost converter with a minimum voltage input around 500 mV. A 100 µF electrolytic capacitor is used to store the BQ25504's output, which is configured to 4.2 V to enable it to drive a WSN based on off-the-shelf components using the energy stored in the capacitor.

The rectenna has been characterized on-body using the setup shown in Fig. 15, where it was mounted directly on the user's chest to include human absorption effects. The incident power S has been varied and the output voltage across the 100 µF capacitor was monitored using an oscilloscope. It was found that the BQ25504 could start from as low as S=0.88 µW/cm^2, where the voltage output is shown in Fig. 17(a). From the charging curve, it can be seen that the capacitor takes approximately 440 s to be charged to 4.2 V. Once the capacitor is fully-charged the RF source is stopped and the stored energy is discharged into a 2.4 GHz WSN based on a TI CC2640 low-power Arm System-on-Chip (SoC) with an on-chip Bluetooth Low Energy (BLE) transceiver. The SoC is programmed to transmit and advertisement packet at 0 dBm, whose current consumption (from shut-down) is shown in Fig. 17(b). The energy stored in the 100 µF capacitor powers the SoC for under 1 s, which is sufficient for a successful BLE advertisment which can be received by a smartphone.

The on-body wireless powering experiment was repeated at varying S to quantify the charging time/S dependency. Fig. 17(c) shows that the on-body charging time, using the proposed low-profile unshielded rectenna, could reduce to 35.3 s for a 5.5 µW/cm^2 incident wave, which was measured at 1.2 m away from approximately 1 W EIRP source. The same experiment has been repeated in the absence of the human body to investigate the human-induced losses. In Fig. 17(c) it can be seen that the sensitivity of the rectenna improves to 0.55 µW/cm^2, which is higher than a previously reported rectenna implemented on a conventional PCB and integrated with the same PMIC, highlighting the high efficiency of the proposed rectenna.

The proposed rectenna is compared to state-of-the-art flexible and textile-based rectennas in Table II. In addition to being the only wearable antenna to employ an HF inductive element for near-field WPT, the proposed antenna maintains a very small form-factor, relative to the frequency of operation, compared to all reported e-textile rectennas. Moreover, the antenna maintains its S_{11} bandwidth over different body parts. Furthermore, owing to the rectifier's high PCE under -15 dBm, the proposed rectenna maintains a high sensitivity to sub-μW/cm^2 power densities, resulting in the maximum measured wireless PCE of over 40% under 0.5 μW/cm^2, in line with that of rectennas designed solely for far-field WPT and occupying a larger area [9]. Moreover, the proposed broadband antenna design is the first to demonstrate that the antenna's bandwidth can be maintained over different substrates with no dependence on the thickness or the dielectric properties, resulting in a textile-based rectenna with under 0.5 mm thickness and fabric-independent performance. Distinguishable from previously-reported wearable rectennas, the proposed rectenna is the first to be demonstrated powering a real-world load, in the form of a PMIC and Bluetooth WSN, on the body from S <1 µW/cm^2.

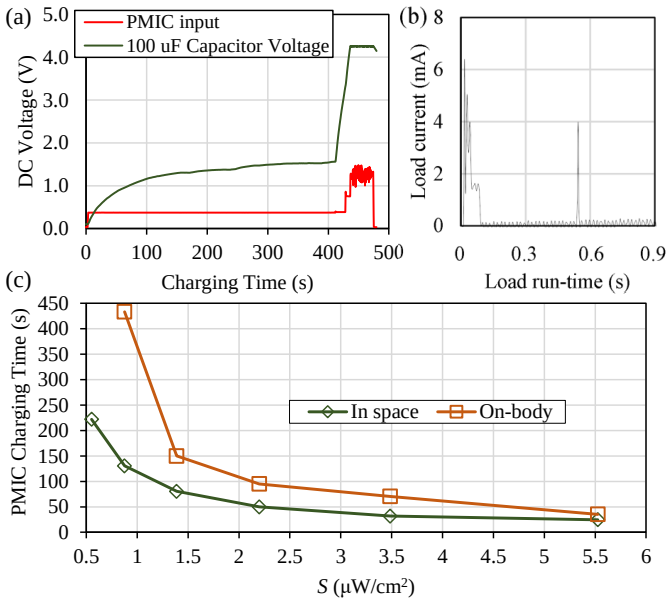

Fig. 17. Measured response of the BQ25504 PMIC powered from on-body RFEH: (a) DC voltage output at S=0.88 µW/cm^2; (b) load current drawn by the BLE node; (c) PMIC+load charging time for varying S.

C. Near-Field WPT Evaluation

The HF MR-WPT efficiency between two similar dual-mode antennas has been characterized experimentally through the $|S_{21}|$ using the VNA. The WPT efficiency was measured for different displacement between the coils, as well as for varying horizontal misalignment. The performance of the proposed antenna is compared to the peak theoretical WPT achievable by conventional symmetric coils, with no UHF radiating elements at the center of the coils, to establish the upper performance bound for the MR-WPT efficiency.

Analytically, the $|S_{21}|$ between two resonant coupled inductors, with a mutual inductance in between, can be calculated

TABLE II
COMPARISON OF THE PROPOSED NEAR- AND FAR-FIELD RECTENNA WITH OTHER WEARABLE RECTENNAS.

Study	Rectenna Substrate	Application	Frequency (GHz)	Gain	Rectifier diode	PCE at −20 dBm (%)	PCE at S=0.5 μW/cm^2 (%)	Electrical size (λ_0^3)
This work	Any fabric (felt and polycotton)	Near and Far-field WPT	HF (6.78 MHz); UHF: 0.86–4.0 GHz	2.2 dBi (in space at 900 MHz); −6.5 dBi (on-body at 900 MHz)	SMS7630-079lf	40±5	42%	0.312× 0.312× 0.0014
2020 [9]	Felt (all fabric)	Far-field WPT	0.82	−4 dBi on-body	SMS7630-079lf	41.8	53	0.329 × 0.329 × 0.0027
2013 [6]	Pile+Jeans (all fabric)	Far-field WPT	0.876	4.6 dBi	HSMS-285X	NR	NR, 45 from 3	0.702 × 0.556 × 0.0088
2018 [24]	Felt (all fabric)	Far-field WPT	2.45	7.3 dBi	SMS7630-079lf	33.6	NR	0.74 × 0.39 × 0.028
2019 [7]	Felt (all fabric)	Far-field WPT	2.4	5 dBi	SMS7630-079lf	18	NR	NR, 0.625 × 0.6 × 0.013†
2020 [8]	Cotton (all fabric)	Far-field WPT	2.0-5.0	−15 dBi*	SMS7630-079lf	NR	<5%§	NR, >1 × 1 × 0.0006‡

*Estimated from the graphs; ** typical patch beamwidth; †antenna only; ‡ estimated from the photographs; § PCE calculated using physical area.

as

$$S_{21}(\omega) = \frac{2jMZ_0\omega}{M^2\omega^2 + [(Z_0+R) + j(\omega L - \frac{1}{j\omega C_{\text{tune}}})]^2}, \quad (4)$$

where R is the series resistance of the coils, Z_0 is the characteristic impedance, set to 50 Ω, and M is the mutual inductance between the inductors [37]. For symmetric rectangular coils, M can be calculated analytically [38], and is given by

$$M = \rho \times \sum_{i=n_{TX}}^{i=1} \sum_{j=n_{RX}}^{j=1} M_{ij} \quad (5)$$

$$M_{ij} = \frac{\mu_0 \pi a_i^2 b_j^2}{2(a_i^2 + b_j^2 + s^2)}(1 + \frac{15}{32}\gamma_{ij}^2 + \frac{315}{1024}\gamma_{ij}^4) \quad (6)$$

$$a_i = b_i = r_{out} - (n_i - 1)(w + p) \quad (7)$$

$$\rho = \frac{4}{\pi^2} \quad (8)$$

$$\gamma_{ij} = 2a_i b_i/(a_i^2 + b_j^2 + z^2)), \quad (9)$$

where a_i and b_i are the radii of the primary and secondary coils, z is the vertical separation between the coils, s is the track separation, and n is the number of turns of each coil [38].

The measured $|S_{21}|$ of the coils is shown in Fig. 18(a), along with the calculated maximum achievable $|S_{21}|$ for similar sized square coils, exclusive of frequency-splitting effects, i.e. assuming ideal adaptive tuning is implemented. From the $|S_{21}|$ measured at 6.78 MHz, f_r for which C_{tune} was calculated, it can be seen that the critical coupling is reached for a separation around 3 cm. In the over-coupling region, the S_{21} at f_r drops due to frequency splitting [37]. Furthermore, observing the peak measured $|S_{21}|$, i.e. assuming adaptive tuning is implemented, it can be seen that the $|S_{21}|$ reaches a maximum of −0.9 dB, corresponding to a link efficiency of 81%. Horizontal misalignment was investigated experimentally at 2.5 cm vertical separation between the coils, where the $|S_{21}|$

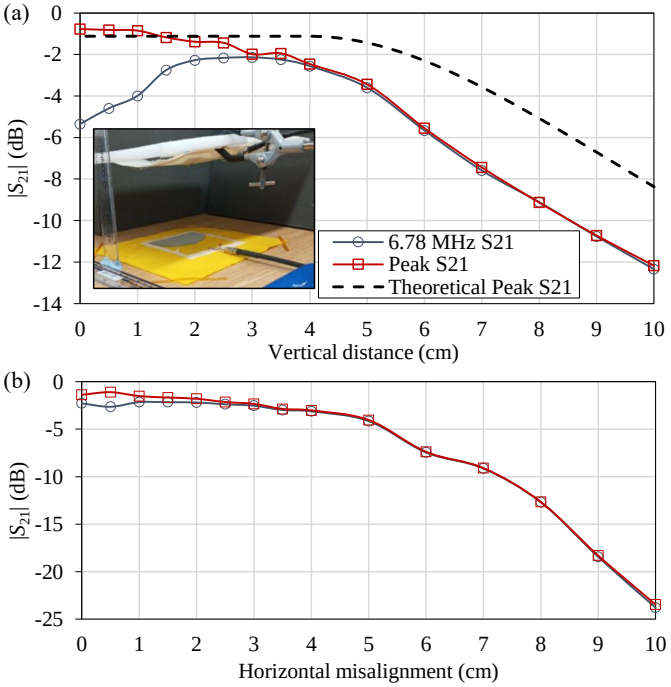

Fig. 18. Calculated and measured forward transmission between the coils at 6.78 MHz and at the frequency corresponding to the maximum efficiency: (a) varying vertical separation; (b) varying horizontal misalignment at 3 cm separation.

is shown in Fig. 19(b). It can be seen that for up to 4 cm misalignment, the $|S_{21}|$ is mostly maintained. The measured performance of the dual-mode antenna is in line with that of unloaded inductors designed solely for near-field MR-WPT.

For a 3 cm separation, i.e. approximately at critical coupling, the frequency domain s-parameters response is shown in Fig. 19. The frequency splitting effect is observed in the $|S_{11}|$ response, where the dual resonant modes are observed. The measured S_{21} response exhibits a wider 3 dB bandwidth

TABLE III
COMPARISON OF THE PROPOSED ANTENNA'S NEAR-FIELD PERFORMANCE WITH OTHER TEXTILE MR-WPT IMPLEMENTATIONS.

	Near-Field WPT Method	Dimensions (cm)	Fabrication	Freq. (MHz)	Substrate	Peak Eff. at 0.5 cm Distance	Efficiency at 2 cm Distance
This Work	MR, single-RX	10.9× 10.9	Embroidered Litz wires	6.78	Felt and poly-cotton	81%*	62%
2021 [39]	MR, single RX	Diameter = 6.8	Knitted copper wire	13.56	Cotton swatch	30%	14%
2020 [13]	MR, dual RX	6×6	Embroidered Litz wires	6.78	poly-cotton	90%	40%
2019 [40]	MR, single RX with resonant loop	Diameter = 3.2	Copper tape epoxied onto textiles	80	polyester	60%	≈25%†
2017 [41]	MR, single RX with resonant loop	Diameter = 9	1 mm wire on textile	6.28 and 9.29	polyester	75%	70%

*Exclusive of frequency splitting effects; †estimated from the graph.

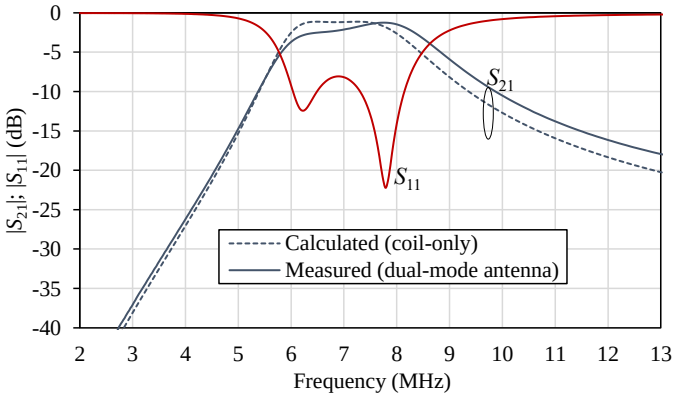

Fig. 19. Calculated (dashed) and measured (solid) s-parameters of the critically-coupled coils at approximately 3 cm separation.

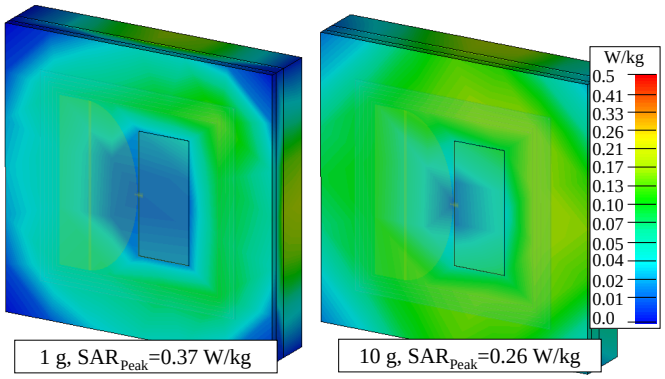

Fig. 20. Simulated SAR distribution for the near-field WPT, at 1 mm from the skin, for a 10 W input.

compared to the theoretical response of single-mode coils, which can be attributed to the lower Q-factor of the inductor after loading with the antenna's UHF radiative elements.

A key advantage of the near-field WPT front-end integrated within the rectenna is the ability to transfer higher power levels to rapidly charge an energy storage device, compared to far-field WPT which is limited to a sub-mW DC power output. The SAR of the proposed antenna, when acting as a near-field power transmitter/receiver has been simulated in CST Microwave Studio, to identify the power levels which can be transmitted/received while complying with the IEEE C95.1 standard. The coil has been simulated at 1 mm away from the skin, in a simplified homogeneous layered tissue model, while coupling to an off-body coil placed at 25 mm vertical separation. The simulated peak S_{21} of -2.4 dB closely approaches the measured S_{21} of -2.2 dB, measured away from the body. This demonstrates that the near-field WPT's efficiency is mostly unaffected by the proximity of human tissue, as well as validates the simulation model. Fig. 20 shows the simulated SAR distribution around the coil (with the off-body coil hidden).

The simulated SAR distribution, for a 10 W input, demonstrates compliance with the 1.7 W/kg peak SAR limit, with a peak SAR under 1.5 W/kg, averaged over 10 gm and 1 gm tissue mass. As the 10 W input was applied at the on-body coil, it is expected that the off-body coil could be excited with a an input over 10 W, to account for the insertion losses in the antenna and in the wireless link. However, such high-power WPT remains dependent on the power handling properties of the embroidered coils.

Table IV-C compares the performance of the antenna as an HF MR-WPT transmitter/receiver to reported flexible and textile-based coils, proposed solely for near-field WPT applications. The proposed antenna achieves a comparable MR-WPT peak efficiency to previous coils which do not have far-field radiative elements. It is noted that apart from [13], the effects of frequency splitting and over-coupling have not been investigated in studies reporting flexible and wearable coils. Considering the state-of-the-art far-field performance, compared in Table II, and the high MR-WPT performance, in Table IV-C, the proposed antenna is highly suited for dual-mode operation.

V. CONCLUSION

In this paper, a dual-mode HF and UHF textile antenna was proposed for simultaneous near and far-field WPT. The proposed antenna combines, for the first time, a broadband UHF radiator with a near-field HF resonant coil. In addition to adding the HF resonant WPT functionality, the inductor

loading the antenna acts a resonator which enables the miniaturization of the broadband monopole. Despite the all-textile simple construction of the near/far-field power harvesting antenna, state-of-the-art performance is demonstrated in both modes of operation in the form of:

- a high maximum achievable near-field wireless power transfer efficiency in excess of 80%;
- a broadband S_{11} bandwidth with a compact antenna, owing to utilizing the coil as a rectangular resonator;
- textile substrate and human proximity-independent bandwidth 135% fractional bandwidth;
- demonstrating a high RF power sensitivity with efficient conversion down to 0.1 μW/cm^2, in line with state-of-the-art far-field-only rectennas;
- harvesting a sufficient DC power output to power a BLE WSN, using a commercial DC-DC converter, from 0.88 μW/cm^2 on-body, despite the lack of a shielding ground plane or reflector.

Based on the proposed antenna, future e-textile wearable devices can be wirelessly powered in both the near- and far-field using a shared-aperture antenna, enabling different charging currents and ranges of operation, for maximum versatility.

ACKNOWLEDGMENT

Datasets supporting this article are accessible from DOI: X.

REFERENCES

[1] X. Lu, P. Wang, D. Niyato, D. I. Kim, and Z. Han, "Wireless Networks With RF Energy Harvesting: A Contemporary Survey," *IEEE Communications Surveys & Tutorials*, vol. 17, 2, pp. 757 – 789, 2015.

[2] C. R. Valenta and G. D. Durgin, "Harvesting Wireless Power: Survey of Energy-Harvester Conversion Efficiency in Far-Field, Wireless Power Transfer Systems," *IEEE Microw. Mag.*, vol. 15, 4, pp. 108–120, 2014.

[3] M. Wagih, A. S. Weddell, and S. Beeby, "Rectennas for RF Energy Harvesting and Wireless Power Transfer: a Review of Antenna Design [Antenna Applications Corner]," *IEEE Antennas Propag. Mag.*, vol. 62 no. 5, pp. 95 – 107, 2020.

[4] D. Marculescu, R. Marculescu, N. Zamora, P. Stanley-Marbell, P. Khosla, S. Park, S. Jayaraman, S. Jung, C. Lauterbach, W. Weber, T. Kirstein, D. Cottet, J. Grzyb, G. Troster, M. Jones, T. Martin, and Z. Nakad, "Electronic textiles: A platform for pervasive computing," *Proceedings of the IEEE*, vol. 91, 12, pp. 1995 – 2018, 2003.

[5] S. Lemey, F. Declercq, and H. Rogier, "Textile Antennas as Hybrid Energy-Harvesting Platforms," *Proceedings of the IEEE*, vol. 102, no. 11, pp. 1833 – 1857, 2014.

[6] G. Monti, L. Corchia, and L. Tarricone, "UHF Wearable Rectenna on Textile Materials," *IEEE Trans. Antennas. Propag.*, vol. 61, 7, pp. 3869 – 3873, 2013.

[7] D. Vital, S. Bhardwaj, and J. L. Volakis, "Textile Based Large Area RF-Power Harvesting System for Wearable Applications," *IEEE Trans. Antennas Propag.*, vol. 68, no. 3, pp. 2323 – 2331, 2019.

[8] J. A. Estrada, E. Kwiatkowski, A. Lpez-Yela, M. Borgos-Garca, D. Segovia-Vargas, T. Barton, and Z. Popovi, "An RF-Harvesting Tightly-Coupled Rectenna Array Tee-Shirt with Greater than Octave Bandwidth," *IEEE Trans. Microw. Theory Techniq.*, vol. 68 no. 9, pp. 3908 – 3919, 2020.

[9] M. Wagih, A. S. Weddell, and S. Beeby, "Omnidirectional Dual-Polarized Low-Profile Textile Rectenna with over 50% Efficiency for Sub-μW/cm^2 Wearable Power Harvesting," *IEEE Transactions on Antennas and Propagation*, vol. 69, no. 5, pp. 2522–2536, 2021.

[10] M. Wagih, N. Hillier, S. Yong, A. S. Weddell, and S. Beeby, "Rf-powered wearable energy harvesting and storage module based on e-textile coplanar waveguide rectenna and supercapacitor," *IEEE Open Journal of Antennas and Propagation*, vol. 2, pp. 302 – 314, 2021.

[11] M. Wagih, G. S. Hilton, A. S. Weddell, and S. Beeby, "Dual-Band Dual-Mode Textile Antenna/Rectenna for Simultaneous Wireless Information and Power Transfer (SWIPT)," *IEEE Trans. Antennas Propag.*, 2021.

[12] A. Hajiaghajani, A. H. A. Zargari, M. Dautta, A. Jimenez, F. Kurdahi, and P. Tseng, "Textile-integrated metamaterials for near-field multibody area networks," *Nat. Electron.*, 2021.

[13] M. Wagih, A. Komolafe, and B. Zaghari, "Dual-Receiver Wearable 6.78 MHz Resonant Inductive Wireless Power Transfer Glove Using Embroidered Textile Coils," *IEEE Access*, vol. 8, pp. 24 630 – 24 642, 2020.

[14] Z. L. Ma, L. J. Jiang, J. Xi, and T. T. Ye, "A single-layer compact hf-uhf dual-band rfid tag antenna," *IEEE Antennas and Wireless Propagation Letters*, vol. 11, pp. 1257–1260, 2012.

[15] M.-S. Wang, Y.-X. Guo, and W. Wu, "Near-field and far-field shared structure for nfc and cnss applications," *IET Microwaves, Antennas & Propagation*, vol. 11, pp. 2116–2123, 2017.

[16] ——, "Planar shared antenna structure for nfc and uhf-rfid reader applications," *IEEE Transactions on Antennas and Propagation*, vol. 65, no. 10, pp. 5583–5588, 2017.

[17] A. Romputtal and C. Phongcharoenpanich, "Iot-linked integrated nfc and dual band uhf/2.45 ghz rfid reader antenna scheme," *IEEE Access*, vol. 7, pp. 177 832–177 843, 2019.

[18] M. Fantuzzi, D. Masotti, and A. Costanzo, "A Novel Integrated UWBUHF One-Port Antenna for Localization and Energy Harvesting," *IEEE Trans. Antennas Propag.*, vol. 63, 9, pp. 3839 – 3848, 2015.

[19] A. Okba, A. Takacs, and H. Aubert, "Compact rectennas for ultra-low-power wireless transmission applications," *IEEE Trans. Microw. Theory Techn.*, vol. 67, 5, pp. 1697 – 1707, 2019.

[20] P. Nepa and H. Rogier, "Wearable Antennas for Off-Body Radio Links at VHF and UHF Bands: Challenges, the state of the art, and future trends below 1 GHz," *IEEE Antennas and Propagation Magazine*, vol. 57 no. 5, pp. 30 – 52, 2015.

[21] M. Wagih, O. Cetinkaya, B. Zaghari, A. S. Weddell, and S. Beeby, "Real-World Performance of Sub-1 GHz and 2.4 GHz Textile Antennas for RF-Powered Body Area Networks," *IEEE Access*, vol. 8, pp. 133 746 – 133 756, 2020.

[22] C. Song, Y. Huang, J. Zhou, P. Carter, S. Yuan, Q. Xu, and Z. Fei, "Matching Network Elimination in Broadband Rectennas for High-Efficiency Wireless Power Transfer and Energy Harvesting," *IEEE Transactions on Industrial Electronics*, vol. 64, 5, pp. 3950 – 3961, 2017.

[23] H. Sun, Y. xin Guo, M. He, and Z. Zhong, "Design of a High-Efficiency 2.45-GHz Rectenna for Low-Input-Power Energy Harvesting," *IEEE Antennas Wireless Propag. Lett.*, vol. 11, pp. 929–932, 2012.

[24] S.-E. Adami, P. Proynov, G. S. Hilton, G. Yang, C. Zhang, D. Zhu, Y. Li, S. P. Beeby, I. J. Craddock, and B. H. Stark, "A Flexible 2.45-GHz Power Harvesting Wristband With Net System Output From -24.3 dBm of RF Power," *IEEE Trans. Microw. Theory Techn.*, vol. 66 no. 1, pp. 380–395, 2018.

[25] Z. Wang, L. Z. Lee, D. Psychoudakis, and J. L. Volakis, "Embroidered multiband body-worn antenna for gsm/pcs/wlan communications," *IEEE Transactions on Antennas and Propagation*, vol. 62, no. 6, pp. 3321–3329, 2014.

[26] J. Liang, C. Chiau, X. Chen, and C. Parini, "Study of a printed circular disc monopole antenna for uwb systems," *IEEE Trans. Antennas Propag.*, vol. 53, no. 11, pp. 3500 – 3504, 2005.

[27] K. P. Ray and Y. Ranga, "Ultrawideband Printed Elliptical Monopole Antennas," *IEEE Trans. Antennas Propag.*, vol. 55 no. 4, pp. 1189 – 1192, 2007.

[28] T. Yang, S.-Y. Suh, R. Nealy, W. Davis, and W. Stutzman, "Compact antennas for uwb applications," *IEEE Aerospace and Electronic Systems Magazine*, vol. 19, no. 5, pp. 16–20, 2004.

[29] J. Liang, C. Chiau, X. Chen, and C. Parini, "Printed circular disc monopole antenna for uwb applications," *Electronics Letters*, vol. 40, no. 20, pp. 1246–1247, 2012.

[30] F. Congedo, G. Monti, L. Tarricone, and M. Cannarile, "Broadband bowtie antenna for rf energy scavenging applications," in *Proceedings of the 5th European Conference on Antennas and Propagation (EUCAP)*, 2011, pp. 335–337.

[31] M. Rossi, S. Agneessens, H. Rogier, and D. V. Ginste, "Assembly-Line-Compatible Electromagnetic Characterization of Wearable Antenna Substrates," *IEEE Antennas and Wireless Propagation Letters*, vol. 16, pp. 1365 – 1368, 2016.

[32] M. Wagih, A. Komolafe, and N. Hillier, "Screen-printable flexible textile-based ultra-broadband millimeter-wave dc-blocking transmission lines based on microstrip-embedded printed capacitors," *IEEE Journal of Microwaves*, vol. 2, no. 1, pp. 162–173, 2022.

[33] R. Del-Rio-Ruiz, J.-M. Lopez-Garde, J. Legarda, S. Lemey, O. Caytan, and H. Rogier, "Reliable lab-scale construction process for electromagnetically coupled textile microstrip patch antennas for the 2.45ghz ism

band," *IEEE Antennas and Wireless Propagation Letters*, vol. 19, no. 1, pp. 153–157, 2020.
[34] J. Bito, J. G. Hester, and M. M. Tentzeris, "Ambient RF Energy Harvesting From a Two-Way Talk Radio for Flexible Wearable Wireless Sensor Devices Utilizing Inkjet Printing Technologies," *IEEE Trans. Microw. Theory Techn.*, vol. 63, 12, pp. 4533–4543, 2015.
[35] A. Alemaryeen and S. Noghanian, "On-Body Low-Profile Textile Antenna With Artificial Magnetic Conductor," *IEEE Trans. Antennas Propag.*, vol. 67 no. 6, pp. 3649 – 3656, 2019.
[36] S. Shen, Y. Zhang, C.-Y. Chiu, and R. Murch, "An Ambient RF Energy Harvesting System Where the Number of Antenna Ports Is Dependent on Frequency," *IEEE Trans. Microw. Theory Techn.*, vol. 67 no. 9, pp. 3821 – 3832, 2019.
[37] T. Imura and Y. Hori, "Maximizing air gap and efficiency of magnetic resonant coupling for wireless power transfer using equivalent circuit and neumann formula," *IEEE Transactions on Industrial Electronics*, vol. 58, no. 10, pp. 4746 – 4752, 2011.
[38] S. Raju, R. Wu, M. Chan, and C. P. Yue, "Modeling of mutual coupling between planar inductors in wireless power applications," *IEEE Transactions on Power Electronics*, vol. 29, no. 1, pp. 481 – 490, 2014.
[39] K. Fobelets, K. Sareen, and K. Thielemans, "Magnetic coupling with 3d knitted helical coils," *Sensors and Actuators A: Physical*, vol. 332, p. 113213, 2021.
[40] K. Bao, C. L. Zekios, and S. V. Georgakopoulos, "A wearable wpt system on flexible substrates," *IEEE Antennas and Wireless Propagation Letters*, vol. 18, no. 5, pp. 931–935, 2019.
[41] S. H. Kang and C. W. Jung, "Textile resonators with thin copper wire for wearable mr-wpt system," *IEEE Microwave and Wireless Components Letters*, vol. 27, no. 1, pp. 91–93, 2017.

Mahmoud Wagih (GS'18, M'21) received his B.Eng. (Hons.) in September 2018, and his Ph.D. on rectenna design in April 2021, both in Electrical and Electronic Engineering from the University of Southampton.

In 2017 he worked as a Research Assistant at the University of Southampton Malaysia. In 2018, he was a Hardware Engineering Intern at Arm, and, in 2020, a Research Intern at Arm, Cambridge, U.K. He is currently a Senior Research Fellow at the University of Southampton, U.K., where he holds a UK IC research fellowship. His interests broadly cover antennas and microwave systems for energy harvesting, sensing, and wearable applications. He has over 55 refereed journal and conference publications, and has delivered several invited webinars on these topics.

Dr. Wagih is a Senior Member of the International Union of Radio Science (URSI) and a member of the Institute of Engineering and Technology (MIET). He is an affiliate member of the IEEE Microwave Theory & Techniques Technical Committees TC-25 and TC-26. He received the Best Student Paper Award at the IEEE Wireless Power Transfer Conference, 2019, the Best Oral Presentation at PowerMEMS, 2019, the Best Paper Award at PowerMEMS, 2021, the URSI Young Scientist Award, 2022, was a Best Student Paper Finalist at IEEE WPTC, 2021, received the IEEE MTT-S Best 3MT Presentation Prize (second place) at the IEEE Microwave Week, 2020, was a U.K. TechWorks Young Engineer of the Year finalist, in 2021, received the URSI Young Scientist Award, 2022, and the EurAAP Per-Simon Kildal Award for the Best PhD in Europe in Antennas and Propagation. He was the recipient of the Best Undergraduate Project Prize, School Winner Doctoral Research Award, Best in Faculty Doctoral Research Award, and the Dean's Award for Early Career Researchers, in 2018-2021, at the University of Southampton. He was a session co-chair at EuCAP, 2021, and a TPC reviewer for various conferences including the IEEE International Microwave Symposium (IMS), and the IEEE Antennas and Propagation Symposium (APS).

Abiodun Komolafe received the B.Sc. degree (Hons.) in physics from the University of Ibadan, Nigeria, in 2007, the M.Sc. degree in microelectromechanical systems, in 2011, and the Ph.D. degree in printed circuits on fabrics from the University of Southampton, in 2016.

He currently works as a Research Fellow with the University of Southampton in investigating novel manufacturing methods for making functional electronics on textiles using flexible electronic circuits and screen-printed electronics for medical applications. He is experienced in the design and fabrication of e-textiles using screen printing and thin-film technologies

Alex S. Weddell (GS'06-M'10) received the M.Eng. degree (1st class honors) and Ph.D. in electronic engineering from the University of Southampton, U.K., in 2005 and 2010.

His main research focus is in the areas of energy harvesting and energy management for future Internet of Things devices. He has over 14 years experience in design and deployment of energy harvesting systems, and has published around 55 peer-reviewed papers in the area. He is currently a Lecturer in the Center for Internet of Things and Pervasive Systems at the University of Southampton, and is involved with three projects funded by EPSRC, EU Horizon 2020 and Clean Sky 2.

Steve Beeby (FIEEE) received the B.Eng. (Hons.) degree in mechanical engineering from the University of Portsmouth, Portsmouth, U.K., in 1992, and the Ph.D. degree in MEMS resonant sensors from the University of Southampton, Southampton, U.K., in 1998.

He is currently the Director of the Centre for Flexible Electronics and E-Textiles and leads the U.K.s E-Textiles Network. He is currently leading three U.K. funded research projects and has received over 20 million research funding. He is a co-founder of Perpetuum Ltd., a University spin-out based upon vibration energy harvesting formed in 2004, Smart Fabric Inks Ltd., and D4 Technology Ltd. He has co-authored/edited four books including Energy Harvesting for Autonomous Systems (Artech House, 2010). He has given over 30 plenary/keynote/invited talks and has over 350 publications and an h-Index of 56. His current research interests focus on energy harvesting, e-textiles and the use of energy harvesting in wearable applications.

Prof. Beeby was the recipient of two prestigious EPSRC Research Fellowships to investigate the combination of screen-printed active materials with micromachined structures and textiles for energy harvesting and was also awarded a Personal Chair in 2011. He has most recently been awarded a prestigious RAEng Chair in Emerging Technologies in E-textile Engineering.